An end-to-end anti-jamming target detection method based on CNN

Yu Zhang, Bo Jiu, *Senior Member, IEEE,* Penghui Wang, Hongwei Liu, *Senior Member, IEEE,* and Siyuan Liang

***Abstract*— Target detection in the presence of main-lobe deception jamming has received intensive attention. Generally, traditional target detection with additive jamming can be regarded as an adjacent process of jamming suppression and target detection. Since target information can be lost in jamming suppression, the detection performance can degrade severely. Aiming at this issue, an end-to-end anti-jamming target detector is proposed based on convolutional neural network (CNN) in the presence of interrupted-sampling repeater jamming. The CNN method first converts the single-pulse compression filter into a series of feature extraction filters, accumulating the energy of various features in various dimensions and on multiple scales. Then, a feature fusion filter added after the feature extraction stage is utilized to suppress jamming features while simultaneously retaining the actual target features. The two stages can be achieved in the CNN structure, and all the filters in this method are obtained by training the CNN. Numerical simulations show the efficiency of the proposed method.**

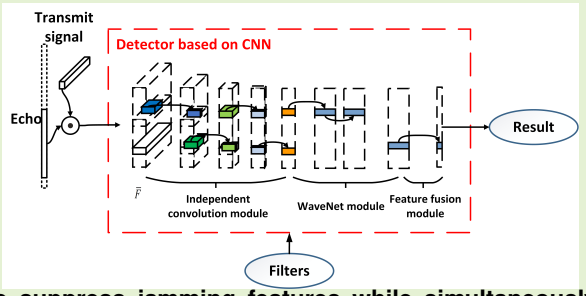

***Index Terms*— target detection, anti-jamming, end-to-end, CNN.**

I. Introduction

THE electromagnetic environment of radar has become increasingly complicated, whereas the use of active jammers has dramatically deteriorated the electromagnetic environment of radar operation. Interrupted-sampling repeater jamming (ISRJ), which is generated by an active jammer, highly matches the radar transmit signal and brings great difficulties to target detection [1]. Given the importance and difficulty of target detection, electronic counter-countermeasures against ISRJ have been extensively studied, among which the issue of target detection in the environment of sidelobe deception jamming has been well solved, whereas target detection in the environment of main-lobe deception jamming is still a hotspot in this field [2].

The latest developments in the field of machine learning, especially the success of convolutional neural networks (CNNs) [3], are dedicated to solving many problems in almost any engineering field, suggesting that data-driven detection methods using machine learning may provide a computationally effective method to achieve near-optimal detection accuracy.

This work was supported in part by the National Natural Science Foundation of China under Grant 61671351, in part by the National Natural Science Foundation of China under Grant 61601340, in part by the National Science Fund for Distinguished Young Scholars under Grant 61525105, in part by the National Science Fund for Distinguished Young Scholars under Grant 62071345, in part by the Natural Science Foundation of Shannxi Province under Grant 2020JQ-297, and in part by the Shaanxi Innovation Team Project.

Yu Zhang, Bo Jiu, Penghui Wang, Hongwei Liu and Siyuan Liang are with the National Laboratory of Radar Signal Processing, Xi'an, China (e-mail: bojiu@xidian.edu.cn, wangpenghui@mail.xidian.edu.cn).

A. Background

Traditional generation of jamming signals is mainly based on analog electronic technology, which requires large equipment and has difficulty guaranteeing accuracy. With the development of science and technology, the generation of jamming signals in electronic warfare has gradually evolved from the early analog mode to the current digital mode. Common technologies for digital jamming generation include digital radio frequency memory (DRFM) [4] and digital jamming synthesis (DJS) [5].

The DRFM jammer generates deceptive jamming signals through two operating modes for the most part: full-pulse-repeat-back mode and interrupted-sampling-repeat-back mode [6]. When the DRFM repetitive jammer operates in full-pulse-repeat-back mode, it will intercept, store and retransmit the entire transmit signal pulse. When using another working mode, the jamming called ISRJ is obtained by sampling the transmitted signal using a rectangular window and retransmitting it multiple times and then repeating this process until the end of the transmitted pulse. It is obvious that the signal retransmitted by a DRFM jammer has a strong correlation with the transmit signal due to the ability to intercept, store and recall radio frequency signals, thus forming a series of false targets in radar after signal processing, such as pulse compression (PC) [7]. In particular, the emergence of ISRJ has greatly limited the ability of target detection.

There are quite a few forms of ISRJs, which can be roughly divided into two categories: normal and modulation.

In the case of normal signals, the sampled signal segments are retransmitted directly, while in the case of modulation, the sampled signal segments need to be modulated and then forwarded. After performing PC on the normal ISRJ, the false target can be obtained [8]. Different from the normal ISRJ, the modulation case can obtain multiple false targets that cover the true target within a large range, causing the radar to ineffectively filter out the false targets [1]. In view of the high energy and wide coverage of the ISRJ, antijamming measures must be taken to enable radar to effectively detect the target. Due to the strong correlation between ISRJ and the transmit signal, many target detection methods, such as pulse-to-pulse waveform agility [9], multipulse coverage [10], frequency agility technology [11], and multicarrier phase-coded technology [12], have failed. Hence, significant efforts have been made by scholars to research methods of target detection against ISRJ.

Most existing anti-ISRJ target detection methods can be sorted into two main classes: "parameter estimation and signal reconstruction" methods and "jamming filtering and target detection" methods. The first class means that the main parameters of the ISRJ are estimated first, and then, the jamming signal and the target signal are reconstructed according to the estimated parameters [13], [14]. Chang Zhou et al. [13] estimated the two key parameters of pulse duration and pulse repeat interval in periodic pulse trains. Chao Zhou et al. [14] estimated parameters such as the intercepted slice width and forwarding times by analyzing time-frequency (TF) characteristics. Then, the jamming signal can be reconstructed with the estimated parameters in the two methods. The above paper uses the "parameter estimation and signal reconstruction" method to reconstruct the jamming signal after estimating the parameters of the ISRJ, which can also be considered a model-based method. However, since jamming characteristics are designed by humans, there is a strong antagonistic purpose. When the actual noise and jamming characteristics do not match the established model or there is a deviation in the parameter estimates, the parameter estimation and signal reconstruction methods can easily cause mismatches, leading to serious degradation in detection performance. The second class suppresses ISRJ by a bandpass filter first and then detects the target by analyzing the pulse compression result [15]–[17]. Gong et al. [15] proposed an effective electronic counter-countermeasure scheme based on the discontinuity of the ISRJ signal in the time domain and constructed a bandpass filter by using the two hyperparameters to filter out the ISRJ signal. In addition, Wei et al. [16] used the method in [15] for wideband radar. However, the performance of the filters constructed in the above two papers depends on the estimation accuracy of the two hyperparameters, and there is a risk of model mismatch. Chen et al. [17] proposed a bandpass filter design method with no hyperparameters through the time-frequency function, which has wider application. It can be seen from the above papers that the "jamming filtering and target detection" method can be divided into two stages, namely, jamming suppression and target detection, which introduces new problems. Specifically, if the target signal and the jamming signal partially overlap, the target information will be lost during the jamming suppression stage and affect the detection performance. In summary, the problems of model mismatch and target information loss occur with the existing methods for anti-ISRJ target detection.

From the perspective of hypothesis testing, the anti-ISRJ target detection problem on each range cell can be regarded as a binary classification problem. Therefore, the target detection problem in the context of main-lobe deception jamming can be modeled using a classifier.

Deep neural networks (DNNs), as powerful classifiers, can well estimate the nonlinear expression of input to output, which is an end-to-end process. In view of its outstanding performance, the DNN has been applied in quite a few fields, such as speech processing, computer vision, natural language processing, image classification and medical image recognition [18]. In these fields, DNN-based methods can surpass the accuracy of human estimation. The excellence of a DNN derives from its ability to extract high-level features after obtaining an effective nonlinear representation of the input space from a large quantity of data using statistical learning methods. This approach is different from previous methods that used manual feature extraction or expert design rules [19]. Although DNNs provide state-of-the-art accuracy on tasks in many fields, it comes at the cost of high computational complexity. Fortunately, there are also some structures in DNN that can extract features well without complicated training, such as CNNs [3]. CNNs use small convolution kernels and dilated convolution structure to extract features, which greatly reduces the number of parameters and helps network training. After each convolution kernel, there is a nonlinear activation unit, which is used to improve the nonlinear expression ability of the network [20]. In fact, deeper CNNs have stronger representation capabilities, so many deep networks such as ImageNet are implemented [21]. However, with the deepening of the network level, the problems of a vanishing gradient and gradient explosion easily occur during training. To address these problems, skip connections and residual connections are proposed. So far, a well-trained CNN-based classifier with excellent nonlinear expression ability can be obtained.

In the field of radar, scholars have used CNNs to complete the feature extraction of various jamming signals and the identification of various jamming signal types, which is part of anti-jamming target detection [22]. The whole target detection process is still multistage, and there is the possibility of target information loss and model mismatch. Therefore, an end-to-end anti-jamming target detection method is urgently needed. In addition, some scholars use CNNs to complete SAR target detection-related work, but this approach is for target detection in SAR images [23].

In fact, the field of radar signal processing is more suitable for target detection on one-dimensional time-domain signals. Therefore, considering the shortcomings of existing anti-jamming target detection methods, target detection can be modeled as a classification task. Therefore, with the powerful nonlinear expression capabilities of CNN-based classifiers, this paper proposes a CNN-based end-to-end anti-ISRJ target detection method.

B. Main contributions

The main contributions of this work can be concluded as follows:

1) This work formulates anti-ISRJ target detection as multiple binary classification problems and proposes a CNN method to achieve end-to-end anti-ISRJ target detection, which integrates feature extraction and target detection.

2) A series of preprocessing methods, such as energy normalization, real-value sequence generation and waveform adaptation processing, are proposed, which solve the problems of complex signals and waveform adaptation in the process of transforming traditional methods to our method.

3) The CNN structure includes jump connections, residual connections and dilated convolutions, which can solve the problems of multiscale feature extraction and long-vector energy accumulation. Numerical simulations show the efficiency of the proposed structure.

The paper is organized as follows. In Section II, the signal model and the working principle of the ISRJ are introduced. Then, anti-ISRJ target detection is presented as a problem of hypothesis testing. In Section III, a method plan is proposed to achieve end-to-end radar target detection. Then, the proposed method is detailed, including the framework, preprocessing, network design and training. In Section IV, numerical simulations are given. Finally, Section V provides concluding remarks.

C. Notation

In this paper, we define the normal distribution as $N(\mu, \sigma^2)$, where μ is the mean and σ is the variance. When considering a complex matrix or vector, its real and imaginary parts are defined as $R(\cdot)$ and $I(\cdot)$, respectively. The i^{th} element of the vector $\mathbf{x}$ will be denoted as x_i, and the elements of the i^{th} row and the j^{th} column in the matrix $\mathbf{X}$ are represented as $X_{i,j}$. The $(\cdot)^{\mathrm{T}}$ indicates transpose. $\lfloor \cdot \rfloor$ means a function that approximates an element to the nearest integer less than or equal to the element.

II. Problem Formulation

A. Radar signal model

Assuming that the radar transmits a random phase-coded waveform, the jamming signals can be obtained based on ISRJ and convolution modulation techniques. An illustration of the working principle of the ISRJ is shown in Fig. 1. First, the jammer samples the radar transmit signal with a rectangular envelope pulse train that has a pulse width of T_w and a repetition period of T_s and then retransmits the slice after convolution modulation and repeats this process until the end of the transmit signal.

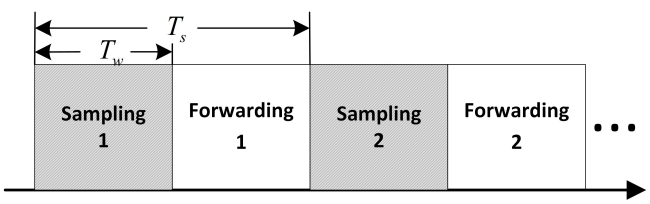

Fig. 1: Diagrammatic drawing of ISRJ.

The random phase-coded waveform $s(t)$ transmitted by pulse radar can be described by the following equation:

$$s(t) = rect(t/T_p)e^{j\phi(t)}e^{j2\pi f_0 t} \tag{1}$$

where

$$rect(\frac{t}{T_p}) = \begin{cases} 1, 0 \le t \le T_p \\ 0, \text{otherwise} \end{cases} \tag{2}$$

is a rectangular window function with pulse width T_p; $\phi(t)$is the phase modulation function, the value range is $0 \sim 2\pi$, and f_0 is the radar carrier frequency.

A rectangular envelope pulse train is utilized to sample the transmit signal, which is recorded as $p(t)$ and can be expressed as [24]:

$$p(t) = rect(\frac{t}{T_w}) * \sum_{n=-\infty}^{+\infty} \delta(t - nT_s) \tag{3}$$

where $*$ is the convolution operation.

The ISRJ with convolution modulation received by radar can be described as:

$$x_j(t) = \left[\left[A_j \frac{[s(t)p(t)] * k}{|[s(t)p(t)] * k|} \right] p(t) \right] * \delta(t - 2R_j/c) \tag{4}$$

where $k(\cdot)$ is the random convolution kernel, R_j is the distance between the jammer and radar, c is the speed of light, and A_j is the amplitude of the jamming signal.

The simplified target echo signal is:

$$x_t(t) = s(t) * \delta(t - 2R_t/c) \tag{5}$$

where R_t is the distance between the target and radar.

The received echo signal contains the target echo signal, the jamming echo signal and noise, which can be described by the following equation:

$$x(t) = x_t(t) + x_j(t) + n(t) \tag{6}$$

Then, the radar performs N_L observations with a time interval of t_s to obtain $\mathbf{t} = [t_s, 2t_s, \cdots, N_L t_s]^{\mathrm{T}}$. The sampled time-domain echo is also obtained, which can be represented as $\mathbf{x} = [x_1, x_2, \cdots, x_l, \cdots, x_{N_L}]^{\mathrm{T}}$, containing the target echo signal, the jamming echo signal and noise, where x_l is the received signal at the l_{th} observation and $[\cdot]^{\mathrm{T}}$ indicates transposition. The sampled transmit signal is $\mathbf{s} = [s_1, s_2, \cdots, s_i, \cdots, s_N]^{\mathrm{T}}$, s_i is the transmit signal at the i^{th} sampling point, and N is the number of sampling points for the transmit signal.

B. Problem description

Anti-ISRJ target detection is essentially a signal detection problem, and it can be described with a hypothesis test. In the binary hypothesis test, H_0 represents the case of a target not present. H_1 represents the case that a target is present. This is the simplest binary hypothesis, in which the two hypotheses H_0 and H_1 are incompatible with each other. The decision regarding these two hypotheses is called binary hypothesis testing.

In the field of pattern recognition, the problem of binary hypothesis testing mentioned above can be regarded as a

binary classification problem. In the classification problem, there are many different ways to use the target value to represent the category label. For probabilistic models, the most convenient method of expression is binary representation [25]. Specifically, there is a target variable $u_i \in \{0, 1\}$, where $u_i = 1$ represents category H_1, $u_i = 0$ represents category H_0, and i is the i^{th} range cell. We can regard the value of u as the probability that the classification result is H_1. For each value in $\mathbf{u} = [u_1, u_2, \cdots, u_i, \cdots, u_L]$, there are two possibilities, namely, there are targets and no targets, and the number of targets is uncertain, so the anti-jamming target detection problem on all range cells can be regarded as multiple binary classification problems.

For the case of binary classification, the posterior probability of category H_1 can be written as:

$$\begin{aligned} P(H_1|\mathbf{x}) &= \frac{P(\mathbf{x}|H_1)P(H_1)}{P(\mathbf{x}|H_1)P(H_1) + P(\mathbf{x}|H_0)P(H_0)} \\ &= \frac{1}{1 + exp(-a)} = sigmoid(a) \end{aligned} \tag{7}$$

where $sigmoid(\cdot)$ is the logistic sigmoid function.

We also define:

$$a = \ln \frac{P(\mathbf{x}|H_1)P(H_1)}{P(\mathbf{x}|H_0)P(H_0)} \tag{8}$$

Note that in (7), we have simply rewritten the posterior probabilities in an equivalent form, so the appearance of the logistic sigmoid may seem rather vacuous. However, it has been proven statistically that regardless of whether an input obeys the Gaussian distribution, an exponential family distribution or is a discrete input, the posterior probability of category H_1 can be written in the form of a logistic sigmoid function acting on a linear function of $\mathbf{x}$:

$$P(H_1|\mathbf{x}) = sigmoid(a(\mathbf{x})) = sigmoid(w^T\mathbf{x}) \tag{9}$$

So far, in this chapter, we have considered classification models that work directly with the original input vector $\mathbf{x}$. However, for many practical problems, the original input vector dimensionality and feature complexity are relatively high, which increases the difficulty of classification in the original observation space. Therefore, we use a parameter adjustable function vector $\Phi(\mathbf{x})$ to perform nonlinear transformations on the input variables to transform the original feature space into a new feature space. The proper nonlinear transformation can make the linearly inseparable categories in the original observation space linearly separable in the new feature space, making the modeling process of the posterior probability easier.

$$P(H_1|\mathbf{x}) = sigmoid(w^T\Phi(\mathbf{x})) \tag{10}$$

For convenience, $\hat{\mathbf{u}} = [\hat{u}_1, \hat{u}_2, \cdots, \hat{u}_i, \cdots, \hat{u}_L]$ will be used to denote $P(H_1|\mathbf{x})$ later, where $\hat{u}_i$ represents the probability that a target exists on the i_{th} range cell. If there is a target in the i_{th} range cell, then we expect $\hat{u}_i$ to be as close to 1 as possible; otherwise, we expect $\hat{u}_i$ to be as close to 0 as possible. For many problems of practical interest, there is significant overlap between the class-conditional densities $p(\mathbf{x}|H_0)$ and $p(\mathbf{x}|H_1)$. This corresponds to posterior probabilities $\hat{\mathbf{u}}$, which, for at least some values of $\hat{\mathbf{u}}$, are not 0 or 1. Therefore, a threshold value l_0 needs to be set here. If $\hat{u}_i$ is greater than l_0, then it is judged that H_1 is true, and if $\hat{u}_i$ is less than l_0, then it is judged that H_0 is true, expressed by the following formula:

$$P(H_1|\mathbf{x}) \underset{H_0}{\overset{H_1}{\gtrless}} l_0 \tag{11}$$

If H_1 is true and the judgment of H_1 is true, then it is called a correct detection. If H_0 is true and the judgment of H_1 is true, then it is called a false alarm. With the two results, the detection probability and false alarm probability can be described by the following equation:

$$P_d = \int_{\{\mathbf{x}:P(H_1|\mathbf{x})>l_0\}} P(\mathbf{x}|H_1)dx \tag{12}$$

$$P_f = \int_{\{\mathbf{x}:P(H_1|\mathbf{x})>l_0\}} P(\mathbf{x}|H_0)dx \tag{13}$$

In equation (13), P_f is a known value; therefore, the threshold l_0, a value between 0 and 1, can be computed by Monte Carlo experiments.

In this section, we model the problem of radar anti-jamming target detection as multiple binary classification tasks. In recent years, CNNs have developed rapidly and have achieved good results in many classification tasks. Therefore, in the next section, we use a CNN for modeling.

III. CNN METHOD

In Section II, anti-ISRJ target detection is described as multiple binary classification tasks. Therefore, in this section, the target detection problem in the context of main-lobe deception jamming is modeled using a CNN-based classifier, which directly outputs the probability of the existence of the target on each range cell to complete the end-to-end integrated detection.

A. Framework

CNN-based anti-jamming target detection can be modeled as the problem shown in Fig. 2. For narrowband radar, the target can be approximated as a point target, and the length of its echo signal depends on the length of the transmit signal. Taking single-pulse detection as an example, assuming that the sampling rate of the radar received signal is equal to the bandwidth of the transmit signal, the radar detection scenario can be discretized into L range cells in units of the range resolution. If the length of the transmit signal vector is N, the length of the received echo vector can be described as $N_L = L + N - 1$.

As shown in Fig. 2, the input of the network is the sampled echo and transmit signal, and the network outputs a vector of dimensions $L \times 1$, where each element value is between 0 and 1, representing the probability of the existence of a target on each range cell. The key to using this new idea to achieve anti-ISRJ target detection is how to design the network structure. Since the end-to-end detection network eliminates many steps

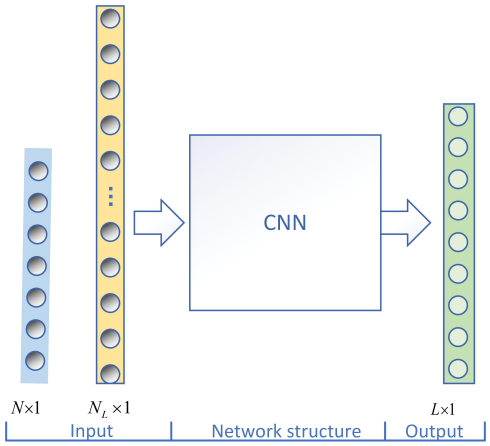

Fig. 2: Basic flowchart of new ideas for anti-jamming target detection.

of traditional radar signal processing, such as ISRJ parameter estimation, anti-ISRJ filter design, and pulse compression, the following issues need to be considered in the design of the network structure.

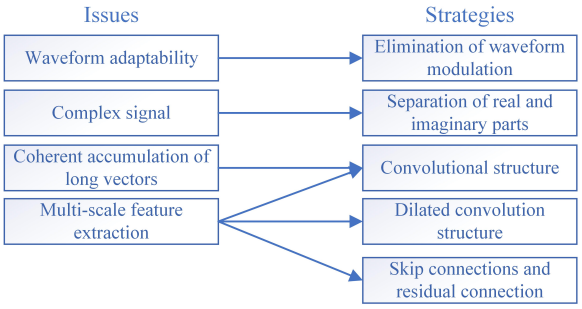

Fig. 3: Issues and strategies.

1) The target echo signal contains the modulated information of the transmit signal. Therefore, how can the network structure be designed to adapt to various waveform modulations?

2) The echo signal is a complex value. In contrast, the network input is a real value. Therefore, how can the radar data be processed to adapt to the network structure?

3) The fundamental guarantee for target detection is signal energy. Therefore, how can the energy accumulation of the echo signal be accomplished?

4) The echo signal vector is usually long. Therefore, how can multidimensional features be extracted to distinguish targets and jamming signals at different scales?

In response to the above problems, the corresponding network structure strategies that we proposed are shown in Fig. 3.

Radar signals and speech signals have highly similar data structures. In speech signal processing, WaveNet, a CNN-based network, has achieved remarkable results [26]. It includes a convolution structure, a dilated convolution structure, skip connections and residual connections. Considering that these structures in WaveNet can be utilized to solve the above issues, we design an anti-ISRJ target detection network structure based on WaveNet, which follows the basic flowchart in Fig. 2. The flowchart of the CNN method is depicted in Fig. 4.

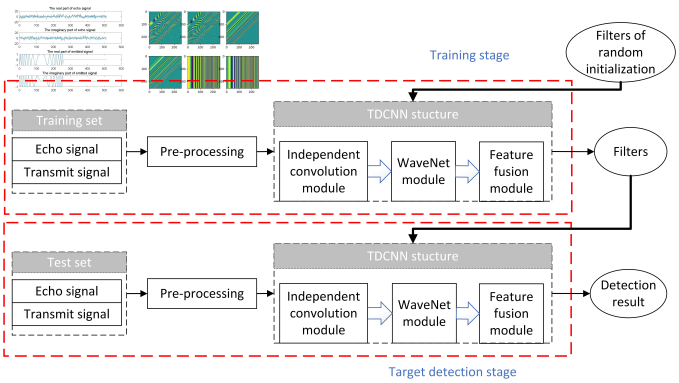

Fig. 4: Flowchart of CNN method.

As Fig. 4 illustrates, the CNN method consists of four main steps:

1) Preprocessing. The echo signal and transmit signal are preprocessed to form the three-dimensional input of the CNN structure, namely, the fast-time dimension, sliding-window-matching dimension and feature dimension, which address the issues of waveform adaptability and complex signals.

2) Independent convolution module. This is the process of using multiple filters with a dilated convolution structure to extract features in the sliding-window-matching dimension and outputting multiple features on each range cell, addressing the energy accumulation issue.

3) WaveNet module. It is used to extract features in the fast-time dimension and continuously update multiple features of each range cell, addressing the multiscale feature extraction issue.

4) Feature fusion module. The multiple features extracted from the fast-time dimension and sliding-window-matching dimension are fused by a filter to form a detection vector, and each element in the detection vector represents the probability that there is a target in this range cell.

B. Preprocessing

The preprocessing involves three steps: energy normalization, waveform adaptation processing and real-value sequence generation, which solves the problems of waveform adaptation and complex signals.

1) Energy normalization

The energy normalization can be expressed by the following formula:

$$\tilde{\mathbf{x}} = \frac{\mathbf{x}}{|\mathbf{x}|_2} \tag{14}$$

where $|\cdot|_2$ is the L2-norm of the vector.

This processing reduces the complexity of the input, which helps network training and avoids gradient explosion.

2) Waveform adaptation processing

According to the relationship between the echo signal and transmitted waveform in the signal model, the modulation

This article has been accepted for publication in IEEE Sensors Journal. This is the author's version which has not been fully edited and
content may change prior to final publication. Citation information: DOI 10.1109/JSEN.2021.3103042

influence of the transmit signal can be eliminated by multiplying the conjugate of the transmit signal and the echo signal of each range cell. The result of the point multiplication is used as a new dimension called the sliding-window-matching dimension, whereas another dimension on the radar echo signal is called the fast-time dimension. An illustration of this process is shown in Fig. 5. This process can be described by the following equations:

$$\mathbf{F}_{1,i,j} = \tilde{\mathbf{x}}_{i+j-1} \times \mathbf{s}_j^* \tag{15}$$

where $i = 1, \cdots, L$ is the label of the fast-time dimension, L is the number of range cells, $j = 1, \cdots, N$ is the label of the sliding-window-matching dimension, N is the number of sampling points for the radar transmit signal, $\bar{\mathbf{F}}_{1,i,j}$ is the first complex feature, and $\mathbf{s}^*$ means the conjugate transpose of $\mathbf{s}$.

Some information about the transmit signal and the echo signal can be lost when performing sliding-window matching, so the characteristics of $\tilde{\mathbf{x}}$ and $\mathbf{s}$ are superimposed.

Then, the second complex feature is obtained by the following equations:

$$\mathbf{F}_{2,i,j} = \tilde{\mathbf{x}}_{i+j-1} \tag{16}$$

The third complex feature is obtained by making the following changes to $\tilde{\mathbf{s}}$:

$$\mathbf{F}_{3,i,j} = \mathbf{s}_j^* \tag{17}$$

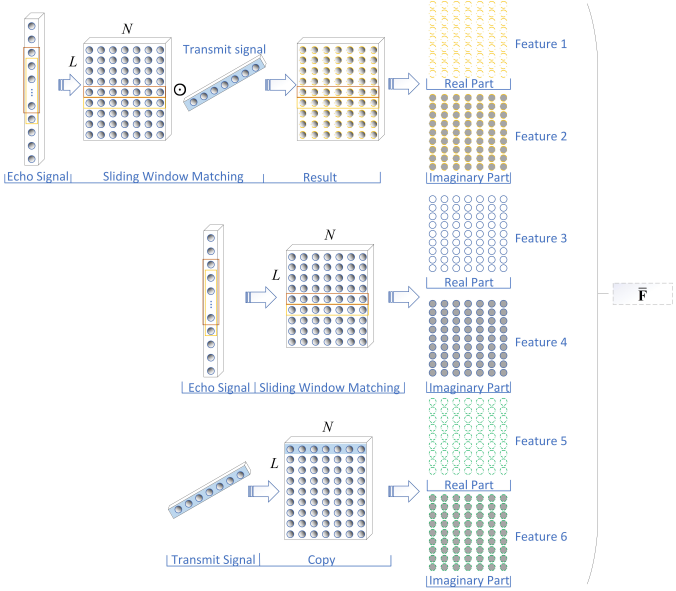

Fig. 5: Schematic diagram of waveform adaptation processing.

3) Real-value sequence generation

Target detection uses signals with complex values, which is less common in CNNs. We address the above three complex features as follows. These six features are stacked together to form a new three-dimensional feature, and it can be represented by $\bar{\mathbf{F}}$, which is the input of the independent convolution module.

$$\bar{\mathbf{F}} = f(\mathbf{s}, \mathbf{x}) = \begin{bmatrix} \bar{\mathbf{F}}_{1,i,j} \\ \bar{\mathbf{F}}_{2,i,j} \\ \bar{\mathbf{F}}_{3,i,j} \\ \bar{\mathbf{F}}_{4,i,j} \\ \bar{\mathbf{F}}_{5,i,j} \\ \bar{\mathbf{F}}_{6,i,j} \end{bmatrix} = \begin{bmatrix} R(\mathbf{F}_{1,i,j}) \\ I(\mathbf{F}_{1,i,j}) \\ R(\mathbf{F}_{2,i,j}) \\ I(\mathbf{F}_{2,i,j}) \\ R(\mathbf{F}_{3,i,j}) \\ I(\mathbf{F}_{3,i,j}) \end{bmatrix} \tag{18}$$

C. Independent convolution module

The purpose of this module is to use dilated convolution kernels to extract features in the sliding-window-matching dimension to achieve energy accumulation in the fast-time dimension. It is composed of four layers, where the output of each layer is the input of the next layer. Each layer can be described by the following equations:

$$\mathbf{H}_0 = \bar{\mathbf{F}} \tag{19}$$

$$\mathbf{H}_k = \rho_1(\mathbf{W}_k \mathbf{H}_{k-1} + \mathbf{b}_k) \tag{20}$$

where $\bar{\mathbf{F}}$ is the output of the preprocessing, $\mathbf{W}$ represents the parameters of the filters in the feature extraction part, $k = 1, 2, 3, 4$, and ρ_1 is the leaky rectified linear unit (ReLU) activation function [27].

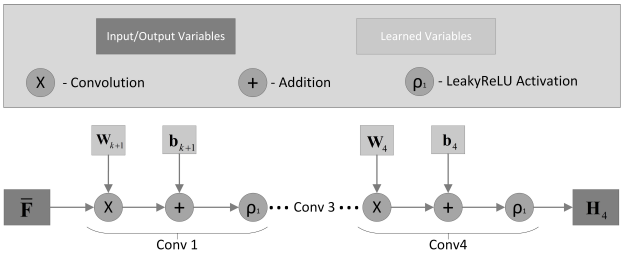

Fig. 6: Detailed diagram of each layer in independent convolution module.

This part uses small filters that have the structure of dilated convolution to extract features in the sliding-window-matching dimension. In CNNs, it is evident that the small-size filters can extract local features, and the dilated convolution can increase the receptive field size, so combining the two can capture global and local dependencies, which is crucial for the feature extraction of filters.

The output of the independent convolution module is multiple feature vectors of the fast-time dimension, which realizes the energy accumulation of each range cell, reduces the influence between different range cells, extracts different features and reduces the dimension of the input data.

D. WaveNet module

The core part of the anti-jamming target detection network uses the WaveNet structure to extract features in the fast-time dimension. As shown in Fig. 7, it contains a dilated convolution, gate activation unit, a convolutional layer with a convolution kernel size of 1, skip connections and residual connections. Dilated convolution has been introduced before,

so the focus is on gate activation units, skip connections and residual connections.

1) Gate activation unit

The gate activation unit similar to the recurrent neural network (RNN) is used in the WaveNet structure [26].

$$\mathbf{Y}_m = \tanh(\mathbf{W}_{h,m} * \mathbf{H}_m) \odot sigmoid(\mathbf{W}_{g,m} * \mathbf{H}_m) \quad (21)$$

where $\odot$ represents the Hadamard product, $sigmoid(\cdot)$ is the sigmoid function, $m = 1, 2, \cdots, 6, 7$ represents the current network layer, h and g represent the filter unit and gate unit, respectively, $\mathbf{W}$ is the learnable convolution filter, $\mathbf{Y}_k$ represents the output of the gate activation unit, and the $\tanh(z)$ and $sigmoid(z)$ activation functions [26].

We can see that the gate activation unit is divided into two parts, namely, the tanh activation part and the sigmoid activation part. The tanh activation part represents the information flowing from the previous layer. The output of the sigmoid activation part is a number from 0-1. It is used to control the proportion of this information layer flowing into the next layer, which is a process of information selection. Applying this structure after each dilated convolutional layer can improve the network's ability to select information so that the network can learn useful information faster.

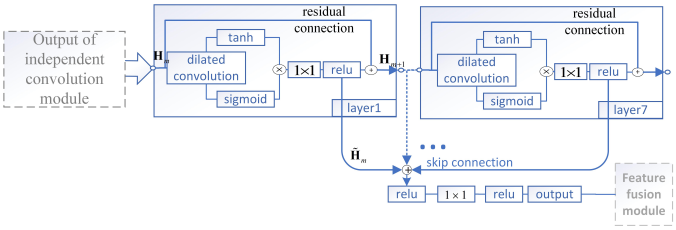

Fig. 7: Schematic diagram of WaveNet.

2) Skip connections and residual connections

In each layer of WaveNet, a residual connection is used, and a skip connection is used between each layer. Adding the input to the output can help deep network training, avoid the vanishing gradient problem, and improve the performance of the network. Specifically, there is a convolutional layer after the gate activation unit, and its convolution kernel size is 1. The residual connection is expressed by the formula as:

$$\tilde{\mathbf{H}}_m = \rho_2(\mathbf{W}_m \mathbf{Y}_m) \quad (22)$$

$$\mathbf{H}_{m+1} = \tilde{\mathbf{H}}_m + \mathbf{H}_m \quad (23)$$

where $\tilde{\mathbf{H}}$ is the output of the convolutional layer after the gate activation unit, $\mathbf{H}_{m+1}$ is the output of the current WaveNet layer, $\mathbf{W}_m$ is the filter parameter, $m = 1, 2, \cdots, 6, 7$, and ρ_2 is the rectified linear unit (ReLU) activation function [27].

Then, the mathematical expression of the skip connection is stated as:

$$\tilde{\mathbf{Y}} = \rho_2(\sum_{m=1}^{6} \tilde{\mathbf{H}}_m) \quad (24)$$

At the end of the WaveNet module, a convolutional layer is used to reselect the information after the skip connection, obtaining the final output of this module, that is:

$$\mathbf{H}_{13} = \rho_2(\mathbf{W}_k * \tilde{\mathbf{Y}}) \quad (25)$$

where $k = 5$.

E. Feature fusion module

After the WaveNet module, there are multiple features in each range cell, and the next problem that needs to be solved is how to select useful features. In this module, we use a convolutional layer with a kernel size of 1 to merge multiple features in the fast-time dimension into one feature, followed by one sigmoid activation function to obtain the detection result on each range cell. This process is described by the following equation:

$$\hat{\mathbf{u}} = sigmoid(\mathbf{W}_k \mathbf{H}_k) \quad (26)$$

where $k = 6$, and $\hat{u}$ is the detection vector.

The network parameters that need to be optimized in the learning phase are:

$$\theta = \{\mathbf{W}_k, \mathbf{W}_{h,m}, \mathbf{W}_{g,m}, \mathbf{W}_m\} \quad (27)$$

where $k = 1, 2, \cdots, 5, 6$, and $m = 1, 2, \cdots, 6, 7$.

Table 1 shows the specific parameters of the network including the layer, output dimensions, trainable parameters and GFLOPs [28]. The next important point is how to obtain the optimal filters to obtain the $\hat{\mathbf{u}}$ for threshold detection, which is detailed in the next section.

F. Training

First, the training set is built for training filters. The parameters in the signal model are selected as follows:

1) The pulse width is $T_p = 43$ ns, the radar carrier frequency is $f_0 = 10$ GHz, the sampling rate is $f_s = 6$ GHz, the pulse repetition interval is 86 ns, the phase at each sampling point is a random number between 0 and 2π. The discrete echo and transmit signal are obtained through the above parameters, the length of the received echo vector is $N_L = 512$, the length of the transmit signal vector is $N = 256$, the range cell is $L = 257$. The range cell where the target is located is randomly selected between 0 and L.

2) The jamming signal x_j is ISRJ with convolution modulation, and the modulation convolution kernel is a gaussian convolution kernel with random amplitude, and the dimension is 1×10, and JSR is a random number between -3 dB and 78 dB, and the range cell where the jamming is located is randomly selected between 0 and L. The number of repetition periods is randomly seleted between 1 and 25, and $\frac{T_w}{T_s}$ is randomly selected between 0.1 and 0.9.

3) $n(t)$ is Gaussian white noise, and the SNR before pulse compression is randomly distributed between -34 dB and 6 dB. The real part of noise is $R[n(t)]$, and the imaginary part of noise is $I[n(t)]$. $R[n(t)]$ and $I[n(t)]$ obey the normal distribution $N(\mu, \sigma^2)$, where $\mu = 0$ and $\sigma^2 = \frac{1}{2 \times \mathrm{SNR}}$.

The radar echo signals are constructed according to the parameters in the above four steps. There are 30,000 groups in the training set, and each group has 64 input-output pairs.

TABLE I: Detailed parameters of network

Layer	Output dimensions	Trainable parameters	GFLOPs
Input	$L \times N \times 6$	-	-
Conv 1 (12 filters, size 1×7, stride 1×3) -LeakyReLU	$L \times \lfloor (N-4)/3 \rfloor \times 12$	516	0.021935089
Conv 2 (18 filters, size 1×7, stride 1×3) -LeakyReLU	$L \times \lfloor (N-16)/9 \rfloor \times 18$	1530	0.020250577
Conv 3 (24 filters, size 1×7, stride 1×3) -LeakyReLU	$L \times \lfloor (N-52)/27 \rfloor \times 24$	3050	0.010887073
Conv 4 (30 filters, size 1×7, stride 1×3) -LeakyReLU	$L \times \lfloor (N-160)/81 \rfloor \times 30$	5070	0.002598241
Polling layer(size $\lfloor (N-160)/81 \rfloor$)	$L \times 30$	0	0.00000768
Conv 5 (64 filters, size 1×1, stride 1×1) -ReLU	$L \times 64$	1984	0.001003265
WaveNet 1 (64 filters, size 3, stride 2^1) -ReLU	$L \times 64$	34167	0.0175
WaveNet ? (64 filters, size 3, stride $2^?$) -ReLU	$L \times 64$	34167	0.0175
WaveNet 7 (64 filters, size 3, stride 2^7) -ReLU	$L \times 64$	34167	0.0175
Conv 6 (1 filter, size 1, stride 1) -Sigmoid	$L \times 1$	65	0.000033153
Total:	-	251383	0.1795

Radar anti-jamming target detection is the case of multiple binary classification in which we have input vectors $\bar{\mathbf{F}}$ and a single target variable $\mathbf{u} = [u_1, u_2, \cdots, u_i, \cdots, u_L]$ such that $u_i = 1$ denotes class H_1 and $u_i = 0$ denotes class H_0. Following the discussion of modeling the problem of radar anti-jamming target detection, the posterior probability of category H_1 can be written in the form of a logistic sigmoid function acting on the linear function of $\mathbf{s}$ and $\mathbf{x}$:

$$P(H_1|\bar{\mathbf{F}}) = \hat{\mathbf{u}}(\bar{\mathbf{F}};\theta) = \sigma(\mathbf{W}_6\Phi(\bar{\mathbf{F}})) \tag{28}$$

where $\bar{\mathbf{F}} = f(\mathbf{s}, \mathbf{x})$, and θ represents the parameters in the network.

Consequently, $0 \leq \hat{\mathbf{u}}(\bar{\mathbf{F}};\theta) \leq 1$. We can interpret $\hat{\mathbf{u}}$ as the conditional probability $P(H_1|\bar{\mathbf{F}})$, with $P(H_0|\bar{\mathbf{F}})$ given by $1 - \hat{\mathbf{u}}$. The conditional distribution of targets given inputs is then a Bernoulli distribution of the form:

$$P(\mathbf{u}|\bar{\mathbf{F}},\theta) = \prod_{i=1}^{L} \hat{u}_i^{u_i}\{1-\hat{u}_i\}^{1-u_i} \tag{29}$$

Taking the negative logarithm of the corresponding likelihood function then gives the following error function:

$$E(\theta) = -\sum_{i=1}^{L}\{u_i \ln \hat{u}_i + (1-u_i)\ln(1-\hat{u}_i)\} \tag{30}$$

We turn next to the task of finding a weight vector θ that minimizes the chosen function $E(\theta)$. The optimized objective function is:

$$\min_{\theta}\{E(\theta)\} \tag{31}$$

The CNN is trained with a variant of the stochastic gradient descent method [29] for optimizing parameters, named the Adam optimizer [30]. All networks are implemented using the Python-based TensorFlow library [31]. The network is trained on the samples of the training set until the error function no longer decreases.

The output of the cross-entropy loss function will be infinite when the independent variable of the logarithmic function in this loss is close to zero. The problem of numerical calculation overflow will occur in the process of actual programming. To solve this problem, a small number is added to the error function.

$$E(\theta) = -\sum_{i=1}^{L}\{u_i \ln(\hat{u}_i + 1^{-10}) + (1-u_i)\ln(1-\hat{u}_i + 1^{-10})\} \tag{32}$$

IV. Simulations

A. Implementation description

To show the performance advantages of this method over other methods and demonstrate how the SNR and JSR conditions affect performance, a series of Monte Carlo simulations were designed [32]. First, the proposed CNN method was compared with traditional methods. The traditional method will be described in detail below. Second, we verified the effectiveness of energy accumulation and waveform adaptation. Third, we used actual measurement data to verify the effectiveness of the method in practical applications. Then, we verified the effectiveness of feature extraction. Finally, visual experiments were performed to show what each layer of the network learned.

Since this method is a brand new idea that has not been previously proposed, we can only compare it with a traditional anti-jamming target detection method, which is divided into four steps: parameter estimation, jamming suppression, PC, and CA-CFAR detection [33]. Specifically, 1) Parameter estimation. The accurate jamming parameters are obtained based on prior knowledge. For any time t during the radar receiving signals, when the target signal is not disturbed by the jamming signal, $\hat{p}(t) = 1$; otherwise, $\hat{p}(t) = 0$, where $\hat{p}(t)$ is the jamming-free segmentation function. 2) Jamming suppression. The jamming-free signal is obtained by extracting segments of signal when the jamming-free segmentation function indicates the signal is jamming-free. 3) PC and CFAR detection. In the jamming suppression stage, a part of the noise energy will be lost. At the same time, if the target and the jamming overlap, the target energy will also be lost to different degrees after the jamming is filtered, which will cause the actual SNR to change.

B. Detection performance

The experiment to verify the detection performance is the detection performance analysis under different SNRs, JSRs and $\frac{T_w}{T_s}$, each of which performs 10,000 repeated Monte Carlo simulations. Specifically, the CNN method in this paper and the traditional method were used for anti-ISRJ target detection when the false alarm probability was 1^{-4}. Then, the probability curves under different SNRs, JSRs and $\frac{T_w}{T_s}$ were obtained.

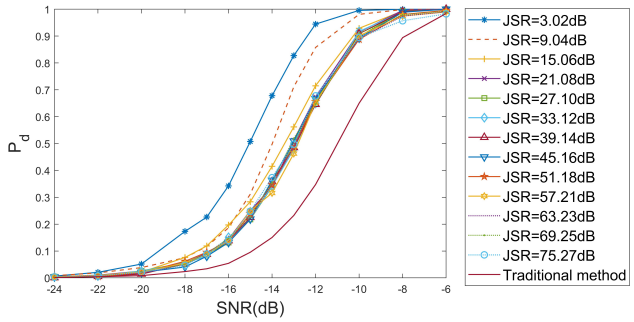

Fig. 8: Detection performance of the two methods under different SNRs and different JSRs and false alarm probability is 1^{-4}, $\frac{T_w}{T_s} = 0.3$.

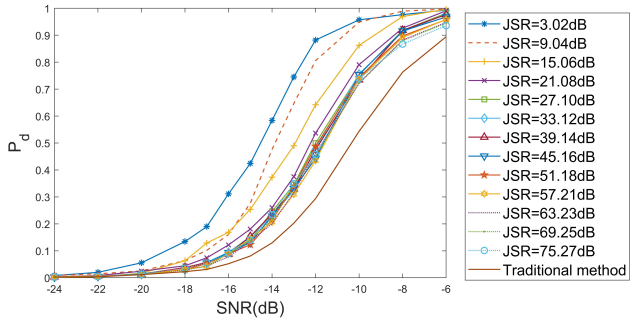

Fig. 9: Detection performance of the two methods under different SNRs and different JSRs and false alarm probability is 1^{-4}, $\frac{T_w}{T_s} = 0.5$.

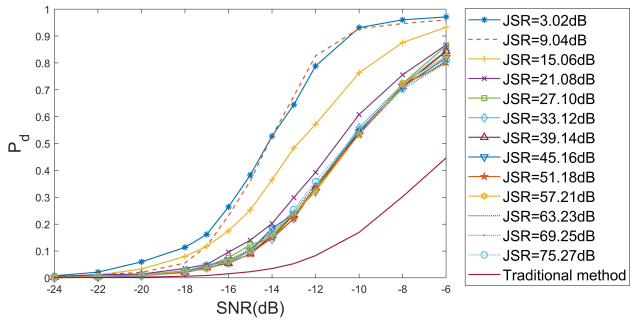

Fig. 10: Detection performance of the two methods under different SNRs and different JSRs and false alarm probability is 1^{-4}, $\frac{T_w}{T_s} = 0.7$.

As illustrated in Fig. 8, Fig. 9 and Fig. 10, the performance of the CNN method is better than that of the traditional method under different SNRs, JSRs and $\frac{T_w}{T_s}$. The higher the SNR, the higher the detection probability. With the increase in JSR, the detection probability of the CNN method decreases and then stabilizes near a value, which is higher than the detection probability of the traditional method. In addition, the reason why the detection probability of the traditional method does not change with the change of JSR is that, when the jamming parameters are known, the SNR loss after multiple Monte Carlo experiments is close to a fixed value, and the SNR loss under different JSRs is basically the same.

C. Effectiveness of waveform adaptation

The purpose of designing waveform adaptation is to eliminate the influence of waveform modulation so that the detection network can complete anti-ISRJ target detection under different transmitted waveforms. To verify the effectiveness of waveform adaptation, the experimental design is as follows.

(1) Random phase coded: the radar transmits a random phase-coded waveform according to the specific parameters mentioned above and then sends the echo signal to the CNN-based detector.

(2) Binary phase coded: the difference in comparison to the random phase-coded waveform is that the radar transmits a binary phase-coded waveform, and the value of phase modulation is 0 or π.

(3) LFM: the radar transmits the LFM waveform, and the complex expression of the LFM waveform at the radar end can be expressed as:

$$s(t) = rect(t/T_p)e^{j\pi Kt^2} \tag{33}$$

where $rect(t/T_p)$ is a rectangular window function with pulse width $T_p = 50$ us; $K = B/T_p$ is the frequency modulation rate; $B = 2$ MHz is the frequency modulation bandwidth.

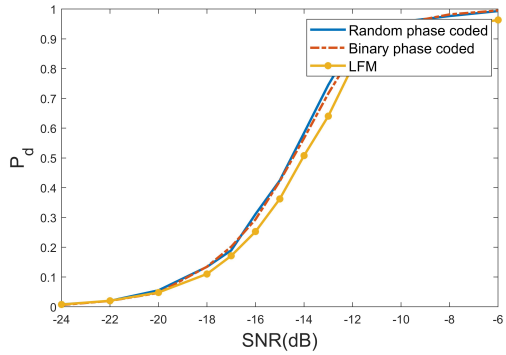

Fig. 11: Detection performance of three transmitted waveforms under different SNRs when JSR is 3dB and false alarm probability is 1^{-4}.

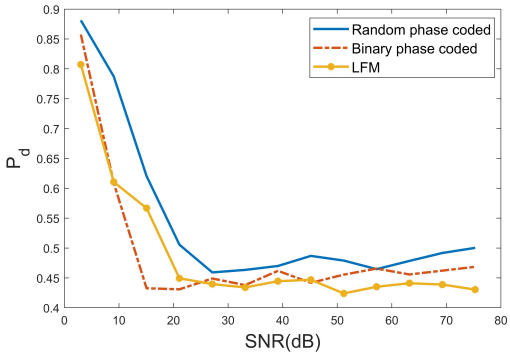

Fig. 12: Detection performance of three transmitted waveforms under different JSRs when SNR is -12dB and false alarm probability is 1^{-4}.

For a given false alarm probability 1^{-4}, the effectiveness of waveform adaptation is evaluated in terms of detection probability, which is estimated through 10,000 Monte Carlo trials. Fig. 11 shows the detection probability curves of the three modulation waveforms under different SNRs, where JSR=3 dB. As Fig. 11 illustrates, the anti-jamming target detection performance under the three waveforms is comparable. In addition, Fig. 12 shows the detection probability curves of three modulation waveforms under different JSRs, where SNR = -12 dB. The results show that the CNN method can adapt to different transmitted waveforms, solving the problem of waveform modulation.

D. Validity in measured signals

There are still some gaps between the radar measured data and the simulated data, so it is necessary to further prove the effectiveness of the method from the detection experiment of the measured data. The signal transmitted by the radar terminal is a linear frequency modulation signal. The radar parameters are shown in the table.

TABLE II: radar parameters

$c/(\mathrm{m/s})$	B/MHz	T_p/us	f_s/MHz	f_0/GHz	P_f
3^8	2	50	5	10	1^{-4}

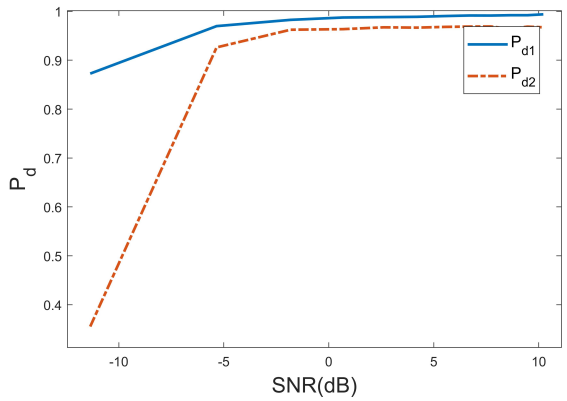

Fig. 13: Detection performance of measured signals under CNN method and traditional method, false alarm probability is 1^{-4}.

There are five types of amplitudes of the transmitted signal: 1, 2, 4, 8, and 12. The jammer adopts the working mode of interrupted-sampling-repeat-back, and the received signal is sampled and doubled and then forwarded. Different from the simulated signal, due to actual equipment, no convolution modulation is done after sampling. Then, noise estimation is performed on the obtained echo signal, and the noise energy in this environment is obtained as 13.69. Then, the SNR under these five transmitted signals is calculated as -11.2816 dB, -5.2610 dB, -0.5948 dB, 6.7802 dB, and 10.3020 dB, and the JSR is 3 dB, where the SNR is after energy accumulation. Target detection on the measured signals under these five SNRs is performed with the CNN method and compared with target detection under the traditional method. The results are shown in Fig. 13, where P_{d1} and P_{d2} represent the detection probability under the CNN method and traditional method, respectively.

E. Effectiveness of the feature extractor

The CNN method is a process of feature extraction and feature fusion, which is the same as the traditional method. The effect of feature extraction determines the performance of target detection. For example, when designing a filter to eliminate jamming in traditional methods, the accuracy of parameter estimation is greatly related to the final target detection performance.

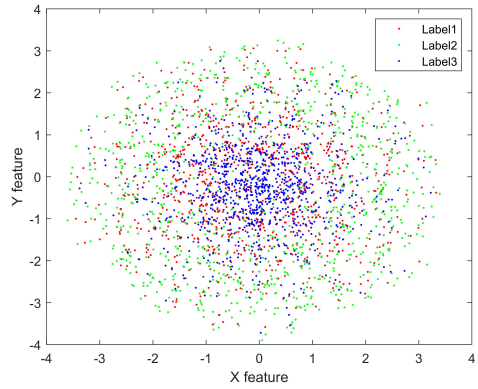

(a)

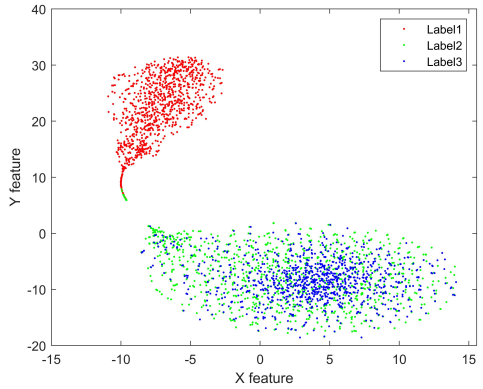

(b)

Fig. 14: The effectiveness of the feature extractor in the CNN method. (a) T-SNE visualization result before feature extraction. (b) T-SNE visualization result after feature extraction.

To understand the effectiveness of feature extraction in the CNN method, the following experiments are designed [34]. We use the T-SNE [35] method to perform dimensionality reduction visualization on 3000 echo samples before network input and after feature extraction. Specifically, the echo samples contain 1000 echo signals with target and noise signals, represented by Label1, 1000 echo signals with jamming and noise signals, represented by Label2, and 1000 echo signals with only noise signals, represented by Label3, where the SNR=-6 dB and JSR=3 dB. Obviously, the method is more

discriminative after feature extraction, which is more helpful for target feature extraction to identify the range cell where the target is located.

F. Visualization of the CNN structure

The purpose of visual analysis is to know what features are learned by the filters in the CNN structure. Gradient-weighted class activation mapping (Grad-CAM) [36] is a class-specific positioning technology that can be extended to any CNN architecture. Considering that the main part of the proposed method is CNN structure, it can be visualized with the Grad-CAM method when the SNR is -6 dB, the JSR is 3 dB and the target range cell is 200. Then, the area and detail features that have a greater impact on the given output are obtained.

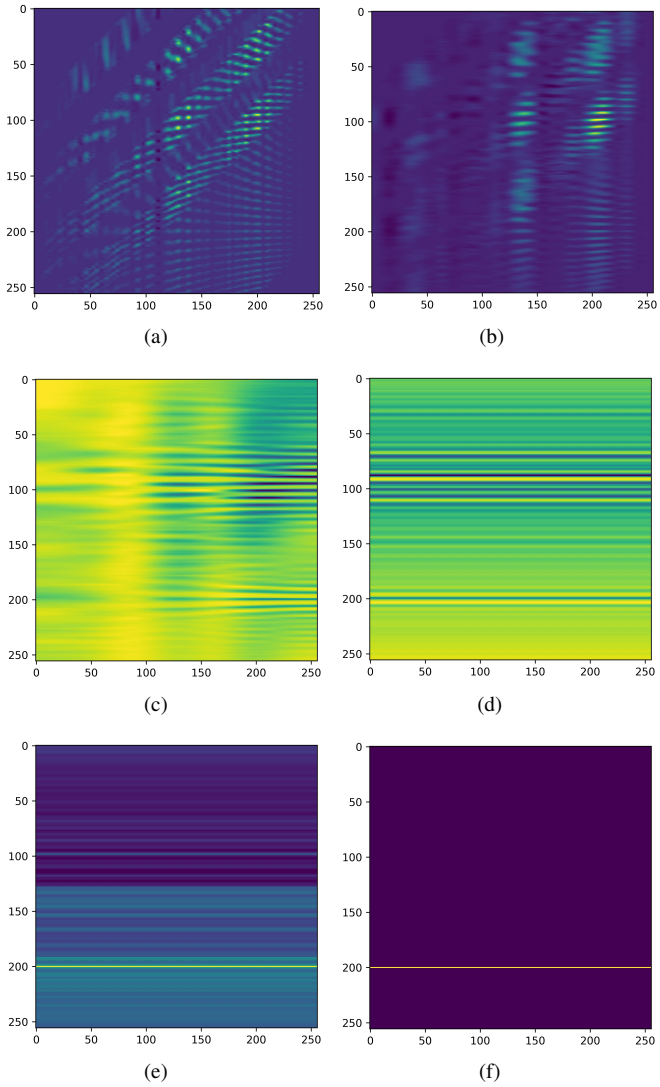

Fig. 15: Grad-CAM visualization of each layer of CNN. (a) Conv1, (b) Conv2, (c) Conv3, (d) Conv4, (e) Conv 5, and (f) Conv 6.

Fig. 15 shows the results of the Grad-CAM visualization method for different feature extraction layers of the CNN structure. It can be seen from the result that the shallow layers are all local features, whereas the deep layers can obtain features with a larger receptive field. As the layer deepens, the heat map pays more attention to the area where the target is located, that is, the 200-range cell. Through visualization, we verified the role of dilated convolution, which can obtain both local and global features. In addition, the filters trained by the network can pay close attention to the range cell where the target is located.

V. Conclusion

We proposed a CNN method and trained it for end-to-end anti-ISRJ target detection, achieving intelligently better detection accuracy under different SNR and JSR conditions, leading to higher real target detection performance than that of the traditional method against ISRJ. Moreover, the proposed method paves a new way for radar to detect and further track and recognize real targets in the ISRJ environment.

The method of anti-ISRJ target detection introduced in this paper is the product of combining radar and artificial intelligence, whereas their combination is not limited to the direction of anti-jamming target detection. Such an approach has profound prospects in intelligent sensors, waveform optimization, and jamming effectiveness evaluation. Therefore, an intelligent radar system can be obtained by combining various parts of the radar with artificial intelligence, thereby improving the battlefield adaptability of electronic warfare systems and shortening the reaction time. These aspects are our research directions in the future. From the current point of view, we will further obtain measured echo data with multiple targets, and improve the network to achieve better anti-jamming target detection performance in the case of multiple targets.

Acknowledgment

This work was supported in part by the National Natural Science Foundation of China under Grant 61671351, in part by the National Natural Science Foundation of China under Grant 61601340, in part by the National Science Fund for Distinguished Young Scholars under Grant 61525105, in part by the National Science Fund for Distinguished Young Scholars under Grant 62071345, in part by the Natural Science Foundation of Shannxi Province under Grant 2020JQ-297, and in part by the Shaanxi Innovation Team Project.

References

[1] C. Li, W. Su, H. Gu, et al, "Improved Interrupted Sampling Repeater Jamming based on DRFM," in: IEEE International Conference on Signal Processing, Communications and Computing (ICSPCC), Guilin, 2014, pp. 254-257.
[2] Qing S, Jian-feng TAO, "Analysis to the Technique of Track-before-detect Anti Radar Main-lobe Interference," DEStech Transactions on Computer Science and Engineering smce, Shanghai, China, 2017.
[3] Chen Yushi, Jiang Hanlu, Li Chunyang, et al, "Deep feature extraction and classification of hyperspectral images based on convolutional neural networks," IEEE Transactions on Geoscience and Remote Sensing, 2016, vol. 54, no. 10, pp. 6232-6251.
[4] S. J. Roome, "Digital radio frequency memory," Electron. Commun. Eng. J, 1990, vol. 2, no. 4, pp. 147-153.
[5] Han Ke, Fuhong Wang, Jianlong Wang, "Research of radar suppression jamming based on DJS," Electronic Science and Technology, 2011.

[6] J. Chen, S. Xu, J. Zou and Z. Chen, "Interrupted-Sampling Repeater Jamming Suppression Based on Stacked Bidirectional Gated Recurrent Unit Network and Infinite Training," in IEEE Access, vol. 7, pp. 107428-107437, 2019.
[7] H. O. Ramp and E. R. Wingrove, "Principles of Pulse Compression," in IRE Transactions on Military Electronics, vol. MIL-5, no. 2, pp. 109-116, April 1961.
[8] D. Feng, L. Xu, W. Wang, et al, "Radar target echo cancellation using interrupted-sampling repeater," IEICE Electron. Exp., 2014, vol. 11, no.8, pp. 1-6.
[9] ZHANG Jindong, LI Sheng, ZHU Xiaohua, "Approach of radar against deception jamming based on waveform diversity," Journal of Data Acquisition and Processing, 2010, vol. 25, no. 2, pp. 138-142.
[10] JIN Shanshan, WANG Chunyang, QIU Cheng, et al, "Design of RF protecting signal for transponder jamming suppression," Journal of CAEIT, 2014, vol. 9, no. 4, pp. 337-381.
[11] LI Yuntao, JIA Xin, CHEN Yongguang, et al, "Frequency agility MIMO-SAR imaging and Anti-deception jamming performance," in: Proceedings of the 31th URSI General Assembly and Scientific Symposium, Beijing, 2014, pp. 1–4.
[12] GUO T, QIU R, "OFDM waveform design compromising spectral nulling, side-lobe suppression and range resolution," in: Proceedings of 2014 IEEE Radar Conference, Cincinnati, USA, 2014, pp. 1424–1429.
[13] Zhou, Chao , F. Q. Shi , and Q. H. Liu, "Research on Parameters Estimation and Suppression for C & I Jamming." International Conference on Radar 2016:1-4.
[14] ZHOU Chao, LIU Quanhua, HU Cheng, "Time-frequency analysis techniques for recognition and suppression of interrupted sampling repeater jamming," Journal of Radars, 2019, vol. 8, no. 1, pp. 100-106.
[15] Gong, Shixian, Xizhang Wei, Xiang Li, "ECCM scheme against interrupted sampling repeater jammer based on time-frequency analysis," Journal of Systems Engineering and Electronics, 2014, vol. 25, no. 6, pp. 996-1003.
[16] X. Wei, G. Zhang, W. Liu, "Efficient filter design against interrupted sampling repeater jamming for wideband radar," EURASIP J. Adv. Signal Process, 2017, vol. 9, pp. 1-12.
[17] J. Chen, W. Wu, S. Xu, et al, "Band pass filter design against interrupted sampling repeater jamming based on time-frequency analysis," IET Radar Sonar and Navigation, 2019, vol. 13, no. 10, pp. 1646-1654.
[18] Minar M R , Naher J,"Recent Advances in Deep Learning: An Overview," 2018.
[19] V. Sze, Y. Chen, T. Yang, et al, "Efficient Processing of Deep Neural Networks: A Tutorial and Survey," Proceedings of the IEEE, 2017, vol. 105, no. 12, pp. 2295-2329.
[20] V. Nair, G. E. Hinton, "Rectified Linear Units Improve Restricted Boltzmann Machines," in ICML, 2010.
[21] A. Krizhevsky, I. Sutskever, G. E. Hinton, "ImageNet Classification with Deep Convolutional Neural Networks," in NIPS, 2012.
[22] Z. Wu, Y. Zhao, Z. Yin and H. Luo, "Jamming signals classification using convolutional neural network," 2017 IEEE International Symposium on Signal Processing and Information Technology (ISSPIT), Bilbao, 2017, pp. 062-067.
[23] X. Tang, X. Zhang, J. Shi, S. Wei and L. Yu, "SAR deception jamming target recognition based on the shadow feature," 2017 25th European Signal Processing Conference (EUSIPCO), Kos, 2017, pp. 2491-2495.
[24] Y. Meng, L. Yu, Y. Wei and P. Tong, "A novel parameter estimation method of interrupted sampling repeater jamming," 2019 IEEE International Conference on Signal, Information and Data Processing (ICSIDP), 2019, pp. 1-5.
[25] Bishop C, "Pattern Recognition and Machine Learning," 2006.
[26] Oord, A. V. D., Dieleman, S., et al, "WaveNet: A Generative Model for Raw Audio," 2016.
[27] V. Nair, G. E. Hinton, "Rectified Linear Units Improve Restricted Boltzmann Machines," in ICML, 2010.
[28] Molchanov, P. , et al. "Pruning Convolutional Neural Networks for Resource Efficient Transfer Learning," 2016.
[29] David E. Rumelhart, Geoffrey E. Hinton, Ronald J. Williams, "Large-scale machine learning with stochastic gradient descent," in: Proceedings of COMPSTAT'2010, Paris France, 2010, pp. 177-186.
[30] Kingma D P, Ba J, "Adam: A Method for Stochastic Optimization," Computer ence, 2014.
[31] Martín Abadi, Ashish Agarwal, et al, "Tensorflow: Large-scale machine learning on heterogeneous distributed systems," 2016, arXiv preprint arXiv:1603.04467.
[32] Chanan Singh, Panida Jirutitijaroen, Joydeep Mitra, "Monte Carlo Simulation," Electric Power Grid Reliability Evaluation: Models and Methods, IEEE, 2019, pp. 165-183.
[33] Mahafza, B. R. ."Radar Systems Analysis and Design Using MATLAB, 3e," CRC Press, Inc.
[34] C. Wang, H. Liu and B. Jiu, "Sliding Residual Network for High-Speed Target Detection in Additive White Gaussian Noise Environments," IEEE Access, 2019, vol. 7, pp. 124925-124936.
[35] K. Kiani, A. Baniasadi, "Speaker Recognition System based on Identity Vector using T-SNE Visualization and Mean-shift Algorithm," in: 2019 5th Iranian Conference on Signal Processing and Intelligent Systems (ICSPIS), Shahrood, Iran, 2019, pp. 1-4.
[36] R. R. Selvaraju, A. Das, R. Vedantam, et al, "Grad-CAM: Why did you say that?," 2016, arXiv preprint arXiv:1611.07450.